JMEPEG (2001) 10:723–730

Mechanisms of Erosion-Corrosion on a Cobalt-Base Alloy and Stainless-Steel UNS S17400 in Aggressive Slurries

M. Reyes and A. Neville

(Submitted 9 April 2001)

Two materials, which are candidates in the construction of drill bits, have been studied in severe liquid-solid impingement conditions. Analysis of the weight loss was carried out on Stellite X40 (Co-base) and UNS S17400 (stainless steel) materials at 30, 60, and 90° angles of impingement under erosion-corrosion conditions at the free-corrosion potential and with applied cathodic protection.

A preliminary analysis of the corrosion behavior of the materials in static conditions was the starting point for the electrochemical analysis. A more extensive corrosion analysis under erosion-corrosion conditions was carried out through direct current (DC) potentiodynamic tests with varying angles of impingement. The results were used to identify the contribution of mechanical erosion and electrochemical corrosion for both materials under different angles of impingement and to determine the extent of interaction between corrosion and mechanical-erosion processes.

Keywords corrosion, erosion, potentiometric tests, Stellite X40, UNS S17400

Introduction and Background

Drilling tools in the oil industry are subjected to severe environments, where highly abrasive rock as well as high rotary speeds and weights can accelerate degradation. It is often assumed that the principal degradation mechanism in offshore drilling is that of the cutting action of the diamond inserts or abrasion caused by the cuttings. However, the problem encountered is not simply a case of high-stress abrasion but also involves erosion-corrosion issues. The presence of corrosive elements in the drilling mud used as lubricants and in the coolants injected at high velocities causes severe wear and erosion in service. The different nozzles direct the mud jets down-hole and sideways onto the bit, cooling it and allowing cuttings to be moved upward. The high velocity of the jet impinging on the side blades degrades the material supporting the diamond inserts.

The drilling jets impinge on the material between and behind the polycrystalline diamond compact (PDC) inserts. The removal of material in the regions behind the PDC inserts causes loss of the materials that support the PDC cutting inserts, as shown in Fig. 1. The working life of a PDC drill bit in subsea can vary from 20 to 200 h depending on the working conditions. The body material currently used is primarily the cobalt-based superalloy Stellite X40. It is common for certain areas of the bit to erode at a high rate, and the diamond cutters are removed due to the loss of support.

M. Reyes and **A. Neville,** Corrosion and Surface Engineering Research Group, Department of Mechanical and Chemical Engineering, Heriot-Watt University, Riccarton EH14 4AS, Edinburgh, Scotland, United Kingdom, Tel 0131 449 5111 Ext. 4365, Fax 0131 451 3129. Contact e-mail: a.neville@hw.ac.uk.

Choosing the correct material for construction of drill bits requires a full understanding of the mechanical properties required and the main mechanisms by which degradation can occur. The requirements for a successful drill bit material are that it can be investment cast, welded, and machined, and has adequate structural properties, such as strength and ductility. The material must also be corrosion and erosion resistant, and economically viable. One potential alternative material to Stellite X40 is UNS S17400 stainless steel, which can be cast and may offer potential benefits in terms of cost.[1]

Erosion-corrosion is a degradation phenomenon that falls into a broad category of tribo-corrosion processes, which includes, *e.g.*, abrasion-corrosion and cavitation-corrosion. These are not specific forms of corrosion but are degradation processes that involve the action of a mechanical process (*e.g.*, an impact of a solid particle) in conjunction with an electrochemical corrosion process. In several works investigating tribo-corrosion processes, such interactions have been identified and quantified.[2–6] They are often classified as "synergistic" or "additive" effects, and in practical terms, these represent an accentuation of degradation due to the combination of mechanical and electrochemical processes. For example, interactions in erosion-corrosion have been identified on aluminum alloys in acidic slurries,[7] on stainless steels in seawater[8] and acidic slurry,[9] and on mild steel in bicarbonate slurries.[10] When materials are exposed to an impinging flow of liquid containing solid particles, the electrochemical response can become complex, involving contributions from impacts and their effects on removal or destruction of protective films.[11] Also, in a recent work,[12] the presence of pitting events superimposed on electrochemical activity caused by impacting solids was identified on stainless steels in saline water.

In this paper, the results from a program to assess the durability of a material currently used in construction of drill bits (Stellite X40) and a possible replacement material (stainless-steel UNS S17400) are presented. Tests have been conducted

under severe erosion-corrosion conditions in order to determine the rates and characterize the main mechanisms of degradation. The importance of the interactions between mechanical processes and electrochemical processes is discussed.

Experimental Procedures

In this study, direct current (DC)-electrochemical accelerated test techniques (potentiostatic and potentiodynamic) were used to assess the corrosion characteristics of the materials under static conditions and while under impingement by a solid-laden aqueous jet.

Static anodic-polarization tests were carried out using a three-electrode cell comprised of an Ag/AgCl reference electrode connected by means of a salt bridge and a platinum counter electrode. The DC anodic-polarization test involved scanning the potential of the working electrode (the specimen under examination) from the free-corrosion potential (E_{corr}) in the more noble (positive) direction at a fixed rate of 25 mV/min. The potential was scanned in the positive direction until the current flow in the external circuit between the working and counter electrodes reached a value of 500 μA/cm^2.

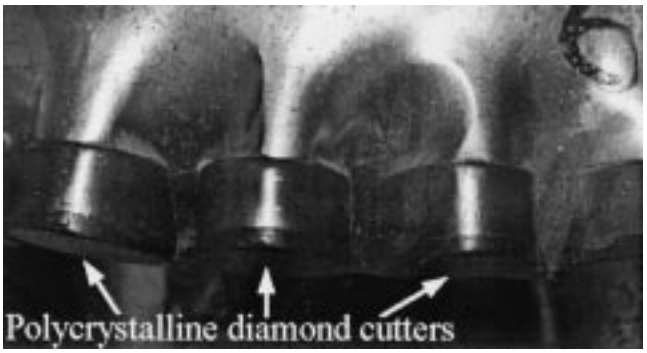

Fig. 1 Severe degradation of the material behind the diamond cutters

The liquid-solid jet was generated using a recirculating rig, as shown in Fig. 2(a). The rig comprised a dual nozzle system. The velocity of the jet for this study was kept constant at 17 m/s. The solid loading in the 3.5% NaCl fluid was maintained at 500 mg/L for all tests referred to in this paper. The silica sand had a size range from 160 to 425 μm with the mean value at 180 μm. The temperature of the liquid was 18 °C. The angle of impingement was varied at 30, 60, and 90°. The anodic-polarization tests were conducted using an *in-situ* three-electrode cell as in the static tests, as shown in Fig. 2(b). The polarization scan was conducted from E_{corr} to the termination current density of 500 μA/cm^2.

In order to isolate the erosion component of material loss, the weight loss was measured after exposure to the impinging jet with applied cathodic protection (CP), which minimized the corrosion current on the sample. The CP was applied by potentiostatic means and involved maintaining the potential of the working electrode at a value of −0.8 V against the saturated calomel electrode (−0.755 V Ag/AgCl).

Following all static and liquid-solid erosion tests, the surface was examined using a light microscope and scanning electron microscope (SEM) to determine the extent of degradation and to identify the material loss mechanisms.

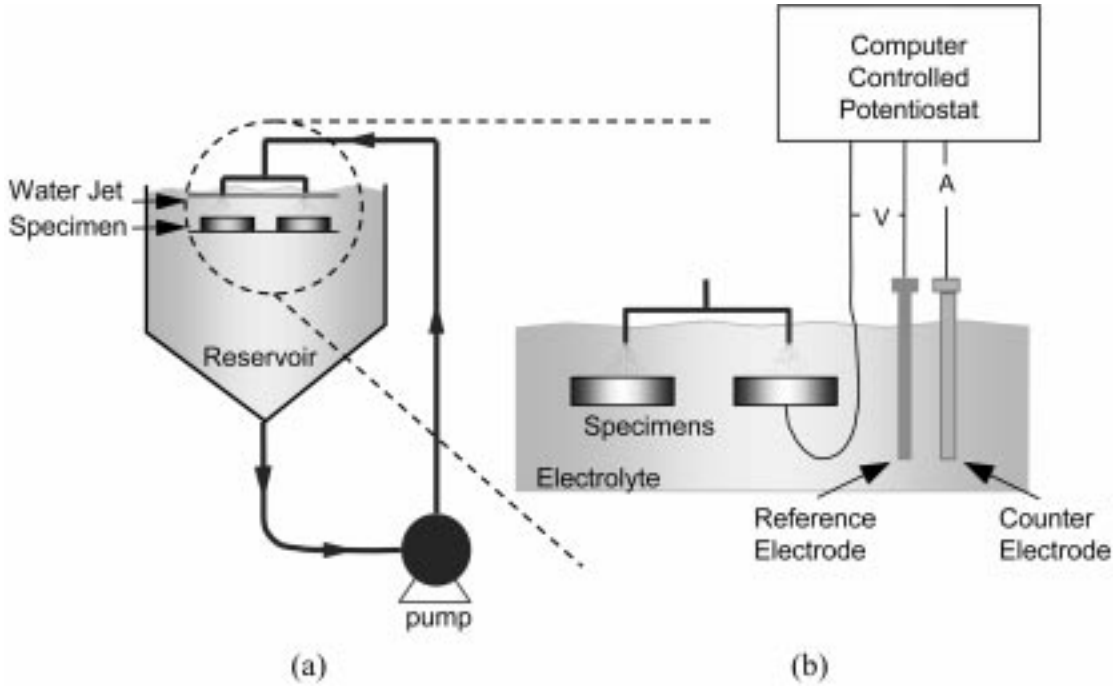

Fig. 2 Recirculating rig with *in-situ* electrochemical monitoring used in erosion-corrosion testing

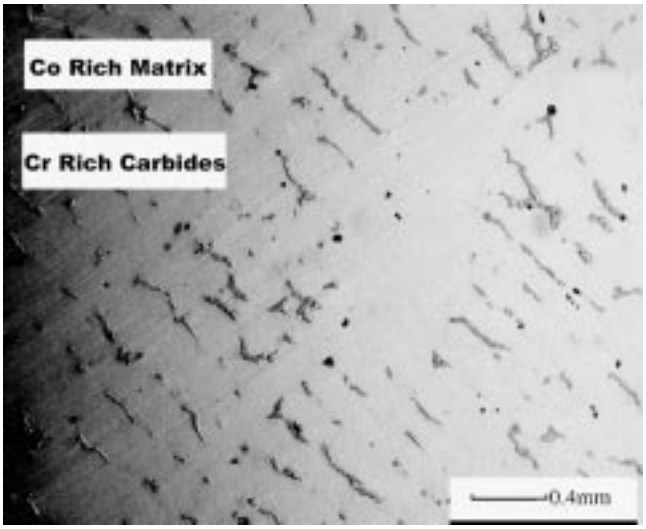

Fig. 3 Microstructure of Stellite X-40 apparent after diamond polishing showing the dentriticlike discrete phase

Table 1 Measured and specified chemical composition of Stellite X40 under 500 mg/L solids slurry erosion changing angle of impingement

Regions of Stellite X40	Cr	Co	Mo	W	Fe	Ni
1 Matrix	24.8	49.4	7.7	7.7	3.7	11.3
2 Hard phase	74	7.2	6.8	6.8	1	0.5
Average analysis	26.9	47.2	8.6	8.6	3.8	10.9
Specified composition	23–30	Bal.	…	6.5–8	5	9.5–11.5

Characterization of Materials

Stellite X40, polished and unetched, has a two-phase microstructure, as can be seen in the light microscope photograph (Fig. 3). The two phases are Cr-rich carbides, and these form a network encapsulated in the Co-rich matrix.

The results of microanalyses measured using the Energy Dispersive X-ray (EDX) attachment on the SEM are given in Table 1. The composition is the average analysis taken over a 600×600 μm square encompassing both phases. The Cr-rich phase (generally known to be carbide) is the constituent of Stellite X40, which confers the hardness and wear resistance. The more ductile "matrix" was found to be higher in Co and slightly denuded in Cr, compared with the bulk analysis.

From Table 1, it is clear that there is generally good correlation between the measured average analysis and that specified by the manufacturer. The hardness of the Stellite X40 was measured as a range from 420 to 555 Hv because of its microstructure of hard carbides dispersed in a softer Co-rich matrix.

The nominal and measured compositions for UNS S17400 obtained by EDAX (without light-element attachment) are presented in Table 2. The microstructure of UNS S17400, shown in Fig. 4, was obtained by electroetching in aqua regia (V2A) (50 mL HCl, 5 mL HNO_3, and 50 mL H_2O). The structure

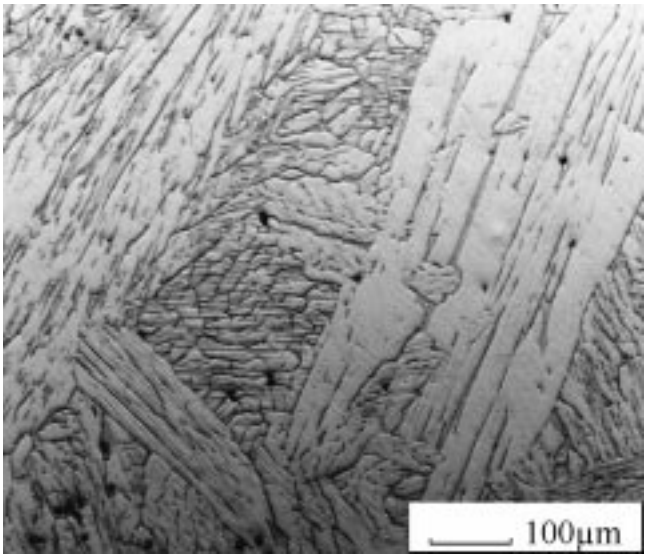

Fig. 4 Microstructure of stainless-steel UNS S17400 polished and etched

comprises grain-boundary precipitation hardening on the lath martensite, which is present in a packet arrangement where the individual laths within the packet have essentially the same orientation. The hardness of the material is 410 Hv.

Results

Static Corrosion Behavior

In the static saline conditions, both materials exhibit passivity, as is evident from the very low currents (typically <5 μA/cm^2), measured as a function of potential in the anodic-polarization curve presented in Fig. 5. The range of potential values over which the materials are passive (marked in Fig. 5 for Stellite X40) are contrasting—in excess of 700 mV for Stellite X40 compared with approximately 200 to 300 mV for UNS S17400. The lower breakdown potential, E_b, signifies a lower resistance of UNS S17400 to the onset of corrosion and the localized loss of passivity. In Table 3, the main mechanisms of corrosion are described, and it is apparent that both materials are affected by localized pitting corrosion. Pitting-initiation sites on Stellite X40 could normally be associated with the interface between the carbide phase and the matrix (Fig. 6), whereas on UNS S17400, no definite correlation with microstructural features could be made.

Corrosion Characteristics under Liquid-Solid Impingement

Figure 7 shows, for the two materials, the anodic-polarization curves recorded during liquid-solid impingement at a 90° angle of impingement. The materials clearly no longer exhibit passivity, and the form of the anodic-polarization plot on both materials is contrasting. The common features on both materials are the increased oscillation in the recorded current when compared with the static anodic-polarization response. In addition,

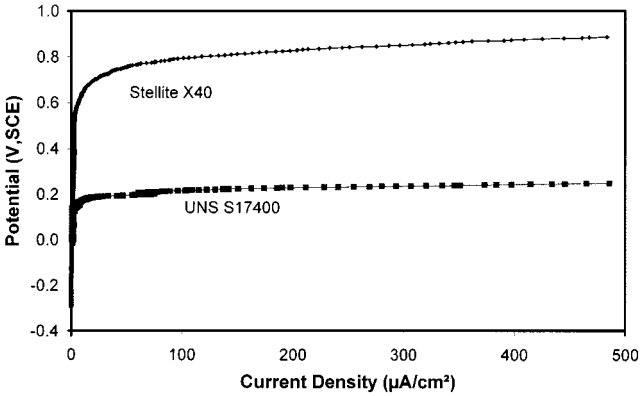

Fig. 5 Static anodic-polarization curves of Stellite X40 and UNS S17400 at 18 °C in seawater

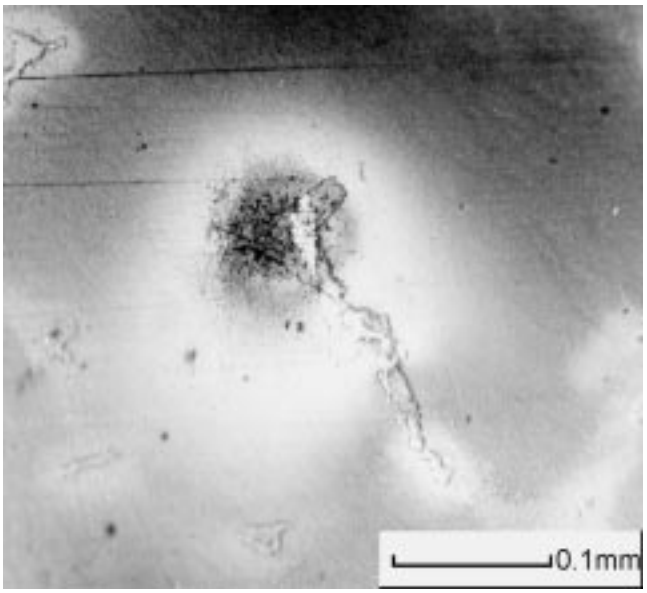

Fig. 6 Stellite X40 after anodic polarization in seawater at 18 °C showing pitting attack at the carbides

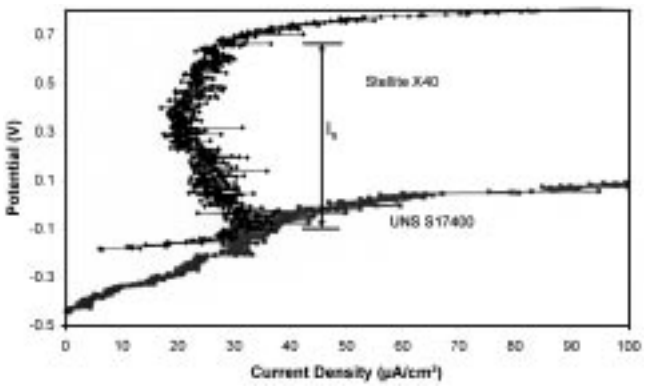

Fig. 7 Anodic polarization under 500 mg/L solids, liquid-solid erosion at 18 °C

the magnitude of current is significantly higher on both materials when compared with static conditions. The main contrasting

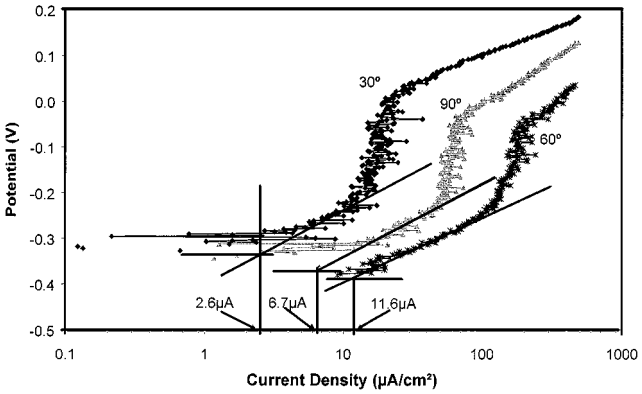

Fig. 8 Anodic-polarization curves under 500 mg/L liquid-solid erosion at 30, 60, and 90° angles of impingement in 3.5% NaCl, 17 m/s at 18 °C for UNS S17400

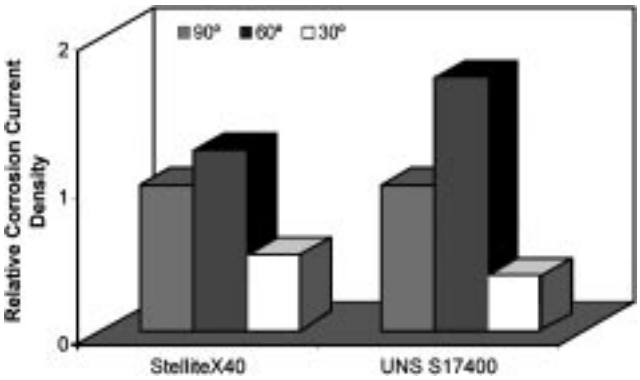

Fig. 9 Corrosion-current density as a function of angle for UNS S17400 and Stellite X-40 normalized to the value at 90°

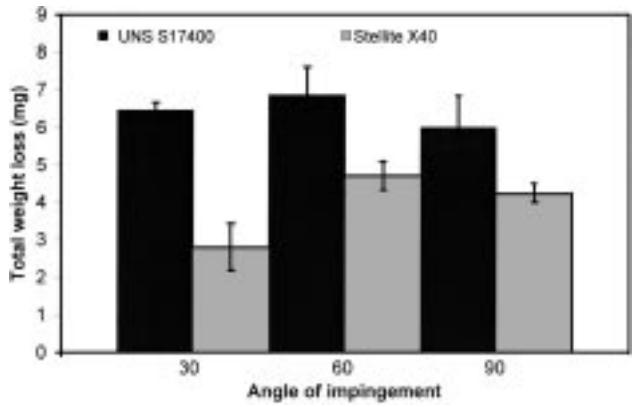

Fig. 10 Total weight loss as a function of angle for UNS S17400 and Stellite X-40

feature is the stabilization of the current after attaining a value of around 30 μA/cm^2 on Stellite X40, labeled I_s in Fig. 7. Immediately on increasing the potential from the free-corrosion potential on UNS S17400, the current increases (following Tafel[13] kinetics), achieving a higher rate of increase once a potential of −0.1 V is reached. This is almost akin to the

Table 2 Nominal and measured chemical composition of UNS S17400

17-4 PH	Cr	Ni	Si	C	Cu	Others
Nominal composition	15.5–17.5	3–5	1	0.04–0.07	3.6	0.25Nb 1Mn 0.04P
Measured composition	16.96	4.15	0.86	6.8	3.52	74.51Fe

Table 3 Description of the mechanisms of attack after anodic polarization in 3.5% NaCl at 18 °C

Material	Type	Attack mechanisms after anodic polarization at 18 °C
Stellite X40	Cobalt-base alloy	Some pitting and pit initiation in the form of concentric colored circles initiating at the carbide/matrix interface. General film over the matrix's phase
UNS S17400	Stainless steel	Most of the area was unaffected, just very few pits and some crevice corrosion

breakdown potential exhibited in static conditions and exhibited at a potential of approximately 0.6 V on Stellite X40 under erosion-corrosion conditions.

From these data, it is possible to calculate the electrochemical corrosion mass loss per unit time using the Tafel extrapolation technique. This is shown clearly in Fig. 8 for UNS S17400 with values of 2.6, 11.6, and 6.7 μA/cm^2 for 30, 60, and 90° angles of impingement, respectively. Figure 9 shows the trends of the corrosion currents of both materials as a function of the impingement angle normalized to the value at 90°. For both materials, the largest value occurs at 60° and the lowest at a 30° angle of impingement.

Measurement of the Total Weight Loss and Its Components

The total weight loss (TWL) is the simplest measure of material degradation and encompasses all the possible degradation mechanisms involving electrochemical processes, mechanical processes, and interaction effects. By analysis of the TWL and the components that constitute the TWL, it is possible to elucidate the factors that have a controlling effect on the material loss.

The important aspects of the material loss as a function of the impingement angle, given as TWL (Fig. 10), are described as follows.

- In common with the electrochemical corrosion results, the maximum TWL value on both materials occurs at a 60° angle of impingement.
- Contrasting trends at higher and lower angles are exhibited such that
  - —on UNS S17400, TWL at 60° > TWL at 30° > TWL at 90°
  - —on Stellite X40, TWL at 60° > TWL at 90° > TWL at 30°.
- UNS S17400 shows smaller changes in TWL as a function of the angle, although TWL values are larger.

Using the corrosion currents obtained during anodic polarization, it is possible to calculate the effect of the angle of impingement on the pure corrosion (C) weight loss component. In addition, the pure erosion (mechanical) component (E) can be measured through application of cathodic protection during liquid-solid impingement and subsequent measurement of weight loss. This enables the synergistic component (S), which is defined as the effect of *corrosion* in accentuating *erosion* to be determined through the arithmetic manipulation of TWL = $E + C + S$. The corrosion material loss (C) in this work is measured *in situ* and encompasses any effects of the flow and solid particles on the corrosion process. The effect of erosion on corrosion is, therefore, accounted for in the assessment of C. Results for UNS S17400 and Stellite X40 are presented in Tables 4 and 5, respectively.

Table 4 Relative contributions of erosion, corrosion, and synergy for different angles on UNS S17400 under liquid-solid erosion of 500 mg/L at 18 °C in 3.5% NaCl

Angle of impingement	*E*%	*C*%	*S*%
30°	56.9	0.8	42.3
60°	53.6	3.5	42.9
90°	66.7	2.7	30.6

Table 5 Relative contributions of erosion, corrosion, and synergy for different angles on Stellite X40 under liquid-solid erosion of 500 mg/L at 18 °C in 3.4% NaCl

Angle of impingement	*E*%	*C*%	*S*%
30°	82.1	2.5	15.4
60°	63.8	3.4	32.8
90°	54.8	3.0	42.2

Both materials exhibit the same characteristic form of wear scar when impinged at 90°, which is in the form of a *w*, as represented in the schematic diagram in Fig. 11(a) and as reported on Stellite X40 in a previous communication.[11] This form of wear scar is in contrast to that observed on cermet materials (Fig. 11b), where the maximum damage occurs in the region directly beneath the jet.[14] Figure 12 shows, for

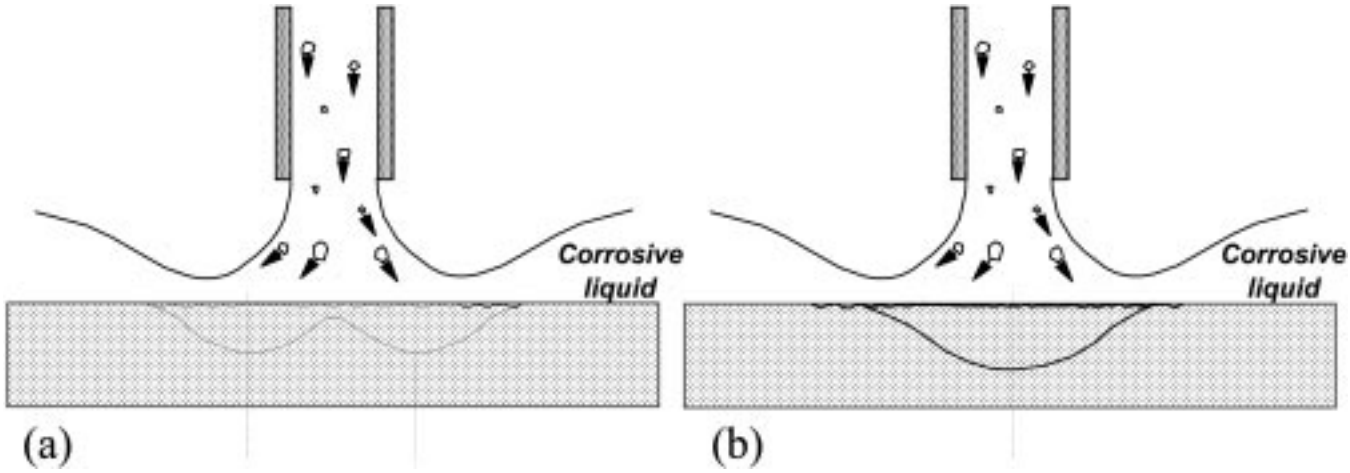

Fig. 11 Schematic representation of the wear scar form on (**a**) Stellite X40 and UNS S17400 in this work and (**b**) cermet coatings studies elsewhere[21]

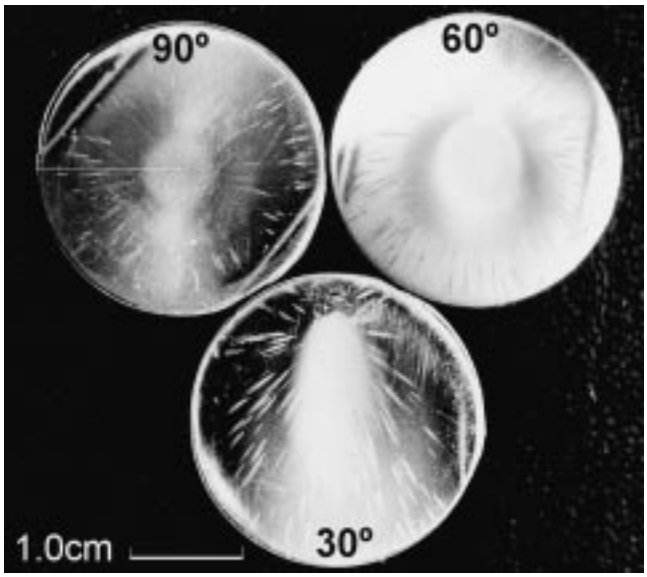

Fig. 12 Wear scars created by anodic polarization under liquid-solid erosion at 30, 60, and 90° angles of impingement for UNS S17400

UNS S17400, the wear-scar region on samples after anodic polarization under liquid-solid impingement. There is a clear change in the geometry of the wear-scar region as the angle of impingement is decreased. The wear scar is elongated in the direction of the flow resulting in an elliptical zone, which is most severely affected by erosion. Inside the central region of the wear scars, little evidence of corrosion attack is seen, and the surface is plastically deformed due to the impacting solid particles (Fig. 13a). Common to all impingement angles is the presence of pits, which appear as cometlike features similar to features reported on stainless steels after anodic polarization under solid-free impingement.[15,16] These tend to be concentrated in the outer zones of the wear scar, where less frequent impacts have occurred and where there is directionality in the mechanical damage (Fig. 13b). A closer view of one of the comet pits is shown in Fig. 14, where the dark pit can be seen and the trailing corrosion products emerging from the pit, which are spreading out radially from the jet direction, are evident.

Pitting is also seen on Stellite X40 after anodic polarization under erosion-corrosion conditions outside the wear scar, being initiated in the carbide/matrix interface. Additionally, in the center of the impingement zone, the two-phase microstructure becomes much more evident due to the variation in hardness between the phases and the preferential erosion of the softer matrix. The network of carbides can be seen, protruding from the surface, at the three angles of impingement after erosion-corrosion for 4 h in Fig. 15.

Discussion

The analyses and comparison of the materials Stellite X40 and UNS S17400 under severe erosion-corrosion environments have identified important aspects relating to their mechanical and electrochemical behavior and the mechanical and electrochemical interactions, which will be discussed further in the following paragraphs.

In this work, three angles of impingement 30, 60, and 90° have been considered. There have been several studies in dry erosion conditions at low and elevated temperature in which the effect of the angle of impingement has been determined, and conclusions about the mode of failure (*i.e.*, ductile/brittle) according to the early work of Finnie[17] have been made. Early work[17,18] predicted that for most metals the maximum solid-particle erosion rate occurred when the particles impacted at shallow angles (*i.e.*, 20 to 30°).

In the work reported in this paper, there are important differences between the two materials, and it is apparent that the maximum erosion-corrosion rate for UNS S17400 occurs at a lower angle (between 30 and 60°) than for Stellite X40 (between 60 and 90°). Nevertheless, the maximum materials loss rate occurs at a much higher angle than that predicted by early solid-particle erosion models. One reason for this may partially lie in the work presented in Sandararajan's second model,[19] where the use of a critical strain criterion was used to predict that, as the type of erodent was changed from angular to

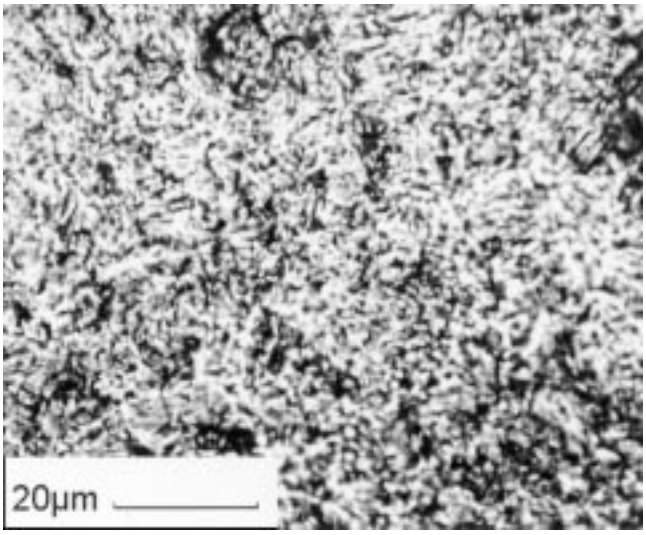

(**a**)

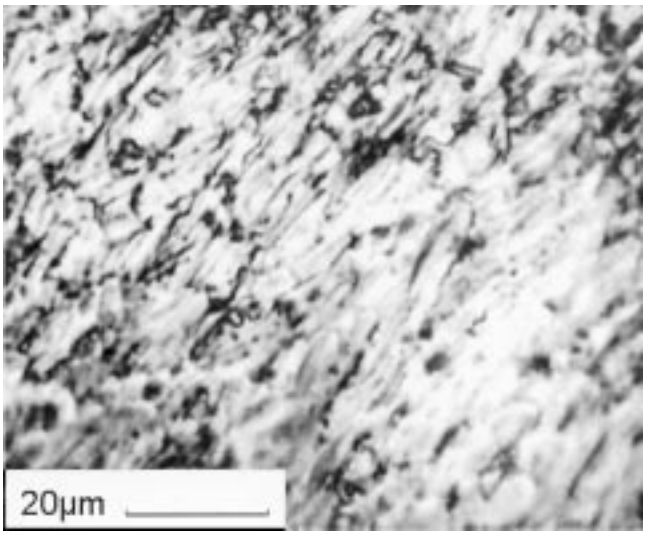

(**b**)

Fig. 13 Surface damage on UNS S17400 in (**a**) the central affected zone of the wear scar and (**b**) outside the central zone

rounded, the angle of maximum erosion shifted to higher values. In addition, the differences between the materials are most probably due to their different microstructures. Stellite X40 has a composite ductile (Co-rich matrix) and brittle (Cr-carbides) microstructure, and it would appear that this is affecting the failure mechanisms. The presence of the brittle carbides is shifting the material loss dependence to higher angles.

Whereas there is still no all-encompassing model to predict the effect of angle on material loss rates in slurry erosion, it is generally agreed that the dependence on angle is a function of the environment and the material type.[20] In agreement with the current study in aqueous sand slurry erosion, work by Zu *et al.*[21] on aluminum alloys recorded a maximum material loss at a much higher angle (50°) than the 20 to 30° predicted from early solid-particle erosion work. Other studies on copper and mild steel have reported similar findings of maximum degradation at an angle less than 90°.[22]

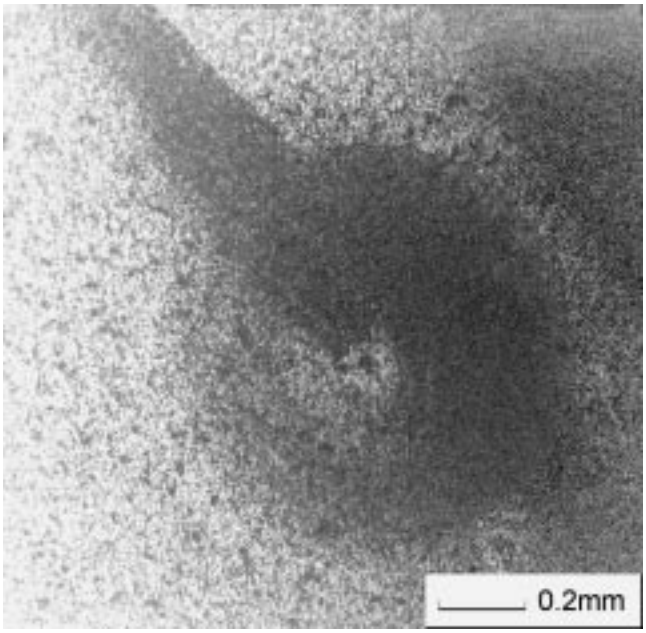

Fig. 14 Pit in the form of a comet developed during anodic polarization under liquid-solid erosion on UNS S17400 at 18 °C and 500 mg/L

In considering angle effects, there is, therefore, much literature where mechanical-erosion mechanisms and rates are modeled. However, it is much less common for corrosion effects as a function of angle to be reported. In this work, although the maximum corrosion rates occur at a 60° angle of impingement for the TWL measurements, there are two main differences between the trends of corrosion and TWL as a function of angle. First, for both materials, there is a higher dependence of corrosion current density on angle than TWL, and second, the maximum corrosion rate for UNS S17400 tends toward higher angles (between 60 and 90°) in contrast to the lower angles for TWL. Under slurry impingement conditions, corrosion occurs (on materials normally passive in static conditions) when the passive film is removed[23] by the impinging solids, and transient-charge transfer can occur. The maximum corrosion rate will most probably occur when the largest area of passive film is removed and the time of impact is greatest. As the angle of impingement changes in slurry impingement, the impacting solid trajectories and the subsequent impact mechanics are changed. At a 90° angle of impingement, the particles impact at a range of velocities and angles, as shown by Benchaita *et al.*[24] For individual impacts at normal incidence, it is expected that there is less charge transfer than at a lower angle due to the ploughing effects of the latter. It is evident from this work that at the most shallow, nominal jet angle, the impacting solids are less efficient in removing the passive film due to the fact that they may not have sufficient energy to penetrate the squeeze film.[25] The corrosion rate being greatest at 60° is an indication that at this angle the optimum balance between the number of impacts and the amount of ploughing is achieved.

The effect of corrosion in terms of electrochemical mass loss in erosion-corrosion is small and, in this work, does not exceed 3.5% of the total material loss. This is higher on lower

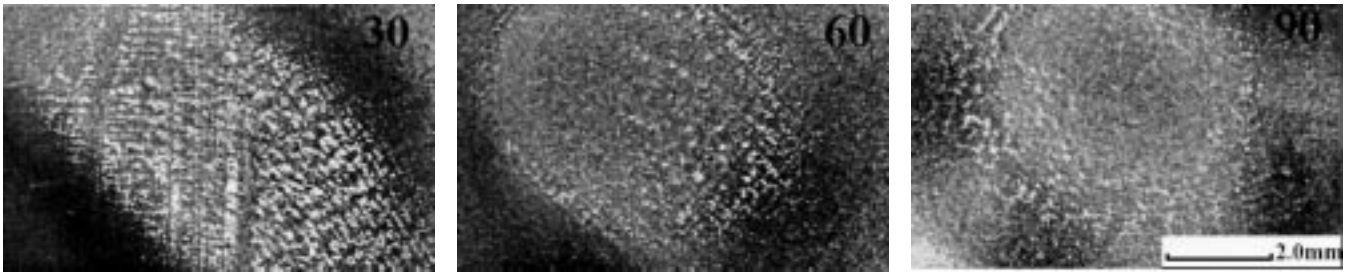

Fig. 15 Wear scars of Stellite X40 under 500 mg/L solids slurry erosion changing angle of impingement

alloy materials (*e.g.*, cast iron[26]). However, of practical and fundamental importance is the indirect effect of corrosion, namely, the synergy. In eliminating corrosion, it is apparent that the total material loss can be reduced by 40 to 45%, implying that corrosion represents a major factor in erosion-corrosion not appreciated through consideration of *C* alone. The relative importance of corrosion is one possible explanation for the inability of researchers to find a single or series of mechanical parameters that could be related to erosion-corrosion resistance. In this study, there is a disproportionate relationship between hardness and erosion-corrosion resistance, although the harder material confers greater resistance in all cases. Although it is generally agreed that increased hardness can often lead to an increased resistance, there has been no unified relationship to relate material hardness to erosion-corrosion resistance.[27]

Practical Considerations

The difference in cost between Stellite X40 and UNS S17400 as castings for drill bits is about 2.5 times ($35.50 per kilo for Stellite X40 and less than $14.20 per kilo for UNS S17400).[1] Achieving an overall cost reduction by changing material is not a simple matter when the data presented in this paper are considered. The difference in TWL can vary from almost 3 times at a 30° angle of impingement to less than 1.5 times at a higher angle. The cost benefits are, therefore, dependent on the regime of erosion-corrosion under which the components operate.

Conclusions

- The resistance of Stellite X40 has been shown to be greater than UNS S17400 under all conditions.
- The total material degradation trend as a function of angle of impingement mimics the corrosion-current density trend on both materials.
- Both materials exhibit passivity in static conditions and active corrosion behavior under erosion-corrosion.
- In practical terms, application of CP to both materials is a viable option for significantly reducing wastage rates.

Acknowledgments

The authors acknowledge financial support provided by BBL Ltd. for MER.

References

1. S. Patel: BBL Ltd., Aberdeen, U.K., private communication, 2000.
2. J. Weber: *Br. Corr. J.*, 1992, vol. 27 (3), pp. 193-99.
3. P. Novak and A. Macenauer: *Corr. Sci.*, 1993, vol. 35 (1–4), pp. 635-40.
4. A. Neville, T. Hodgkiess, and J.T. Dallas: *Wear,* 1995, vol. 186–187, pp. 497-507.
5. M.M. Stack, J. Chacon-Nava, and F.H. Stott: *Wear,* 1995, vol. 180, pp. 91-99.
6. A. Neville, T. Hodgkiess, and H. Xu: *Wear,* 1999, vol. 233–235, pp. 523-34.
7. Y. Li, G.T. Burstein, and I.M. Hutchings: *Wear,* 1995, vol. 186–187, pp. 515-22.
8. A. Neville and T. Hodgkiess: *Br. Corr. J.*, 1997, vol. 32 (3), pp. 197-207.
9. Y. Zheng, Z. Yao, X. Wei, and W. Ke: *Wear,* 1995, vol. 186–187, pp. 555-61.
10. S. Zhou, M.M. Stack, and R.C. Newman: *Corr. Sci.*, 1996, vol. 38 (7), pp. 1071-84.
11. A. Neville, M. Reyes, T. Hodgkiess, and A. Gledhill: *Wear,* 2000, vol. 238, pp. 138-50.
12. G.T. Burstein and K. Sasaki: *Corr. Sci.*, 2000, vol. 42, pp. 841-60.
13. J.C. Scully: *The Fundamentals of Corrosion*, Pergamon Press, Oxford, United Kingdom, 1990.
14. S. Shrestha, T. Hodgkiess, and A. Neville: *J. Thermal Spray Coatings*, in press, 2001.
15. A. Neville and T. Hodgkiess: *Corr. Sci.*, 1996, vol. 38 (6), pp. 927-56.
16. A. Neville: Ph.D. Thesis, University of Glasgow, Glasgow, 1995.
17. I. Finnie: *Wear,* 1960, vol. 3, pp. 87-103.
18. I.M. Hutchings: *Tribology: Friction and Wear of Engineering Materials*, Edward Arnold, London, 1992.
19. G. Sandararajan: *Wear,* 1991, vol. 149, pp. 111-27.
20. J.B. Zu, G.T. Burstein, and I.M. Hutchings: *Wear,* 1991, vol. 149, pp. 73-84.
21. J.B. Zu, I.M. Hutchings, and G.T. Burstein: *Wear,* 1990, vol. 140, pp. 331-44.
22. A.V. Levy and P. Crook: *Wear,* 1991, vol. 151, p. 337.
23. X. Hu and A. Neville: *Werkst. Corr. (Mater. Corr.),* in press, 2001.
24. M.T. Bechaita, P. Griffith, and E. Rabinowicz: *Wear,* 1983, vol. 105, pp. 215-22.
25. H. McI Clark: *Wear,* 1993, vol. 162-164, pp. 669-78.
26. A. Neville, T. Hodgkiess, and H. Xu: *Wear,* 1999, vol. 235, pp. 523-634.
27. *ASM Metals Handbook,* vol. 10, *Liquid-Erosion Failures,* F.G. Hammitt and F.J. Heymann, eds., ASM, Materials Park, OH, 1975.